Research Square

Preprints are preliminary reports that have not undergone peer review.
They should not be considered conclusive, used to inform clinical practice,
or referenced by the media as validated information.

Benchmarking the load-bearing capacity and deformation behavior of an experimental Nb-1Zr dental implant against a commercial Ti-Zr implant system after artificial aging

Karolina Petsa

Petsa.Karolina@mh-hannover.de

Medizinische Hochschule Hannover

Julian-Tobias Schleich

Leibniz University Hannover

Christian Klose

Leibniz University Hannover

Neele Berg-Brümmer

Medizinische Hochschule Hannover

Maren Prediger

Leibniz University Hannover

Hans Jürgen Maier

Leibniz University Hannover

Meike Stiesch

Medizinische Hochschule Hannover

Philipp-Cornelius Pott

Medizinische Hochschule Hannover

Research Article

Keywords: Niobium, Dental Implant, Load-bearing capacity, artificial aging; deformation analysis; titanium-zirconium implant

Posted Date: November 4th, 2026

DOI: https://doi.org/10.21203/rs.3.rs-11385531/v1

License: This work is licensed under a Creative Commons Attribution 4.0 International License.
Read Full License

Additional Declarations: No competing interests reported.

Abstract

Purpose

This study aimed to benchmark the load-bearing capacity and deformation behavior of an experimental Nb-1Zr dental implant against a form-identical experimental implant made of Ti-6Al-4V compared to a commercially established Ti-Zr implant system after artificial aging.

Methods

Twenty-four implant-abutment-crown assemblies (n = 8 per group) were subjected to chewing simulation (1×10^6 cycles, 25 N) and thermocycling (4×10^3 cycles, 5–55°C). Subsequently, all specimens were loaded axially until failure in a universal testing machine. Three-dimensional deviations were quantified by scan superimposition at the implant shoulder and two abutment levels.

Results

All specimens survived artificial aging. Mean maximum failure loads were 2595 N ± 1068 N for Nb-1Zr, 2358 N ± 1057 N for Ti-6Al-4V, and 3743 N ± 201 N for the commercial Ti-Zr implant system. The commercial system showed significantly higher F_{max} than both experimental groups. In contrast, three-dimensional analysis revealed significantly higher abutment-level deformation in the commercial group ($p \leq 0.002$), whereas shoulder-level deviations remained low across groups.

Conclusions

The experimental Nb-1Zr implant exceeded clinically relevant force thresholds and performed comparably to form-identical Ti-6Al-4V. Benchmarking against a commercial Ti-Zr implant system revealed higher ultimate load-bearing capacity of the commercial system.

1 Introduction

Dental implants are an indispensable treatment option for both fixed and removable dental prostheses. Despite high survival rates, implants are still associated with complications that are clinically significant. Among biological complications, peri-implant inflammatory diseases are the most common, while mechanical complications include screw loosening, component deformation, and fractures of superstructures or implant-abutment elements, particularly in cases of high occlusal loads and parafunctional habits [1].

From a materials science perspective, titanium and titanium alloys - particularly Ti-6Al-4V - have long been considered the standard of care due to their favorable mechanical properties and clinical track

record. However, attention is increasingly turning to potential material-related factors that contribute to periimplant inflammation and adverse tissue reactions. In particular, titanium particles and ions can be released during implantation, function, maintenance procedures, and tribocorrosion processes; their distribution in the peri-implant tissue and their potential contribution to inflammatory processes are currently the subject of ongoing discussion [1–4]. While causality remains complex and clinical evidence is heterogeneous, these concerns continue to motivate the search for alternative implant materials with high mechanical stability and improved biological profiles [1, 5, 6].

Niobium-based metallic biomaterials represent a promising class of alternative implant materials. Recent review articles highlight their favorable corrosion resistance in biological media, their promising cell and tissue compatibility, and potential benefits for bone formation, which depend on the alloy composition and fabrication methods [3, 7, 8]. In dentistry, such alloys are particularly attractive because implant materials are exposed to a demanding oral environment characterized by fluctuating pH levels, temperature fluctuations, and mechanical stress. Furthermore, care can be taken in the alloy composition to avoid elements whose long-term biocompatibility is controversial.

Beyond bulk material selection, implant system performance is strongly shaped by macro-design and the implant-abutment connection. The connection geometry influences mechanical stability, micromovements, and the risk of microleakage at the interface-factors that link mechanical behavior with biological outcomes. Recent experimental and evidence-synthesizing work suggests that conical connection designs can provide improved stability under cyclic loading and may reduce microleakage compared with internal hexagon connections, and that connection geometry affects abutment screw stability under cyclic loading [9, 10]. Consequently, a clinically meaningful evaluation of novel materials and designs requires comparisons not only against form-identical experimental controls but also benchmarking against commercial assemblies.

In our previously published in vitro study, the load-bearing capacity of an experimental Nb-1Zr dental implant was investigated in comparison to a form identical Ti-6Al-4V implant, using chewing simulation for artificial aging followed by a load test to failure [11]. Because parafunctional bite forces may approach approximately 800 N and bruxism has been associated with increased implant failure risk, this threshold was used as a clinically relevant reference value [12, 13]. The presented study demonstrated that both experimental implant materials exceeded clinically relevant force thresholds. Within the DFG-funded SFB/TRR 298 SIIRI project, the experimental implant is envisioned as an infection-reactive dental implant. This implant is envisioned to combine mechanical stability with the potential for controlled local release of anti-infective or anti-inflammatory agents from the inside of the implant via a special channel system and a special surface coating to ensure a pump controlled and targeted distribution of the drug into the surrounding tissue.

All of the nowadays-existing experimental implant prototypes were manufactured at Institut für Werkstoffkunde at Leibniz University Hannover. However, the previous study did not address how the experimental implant performs in comparison to an optimized, commercially established implant

system. This limits the translational interpretation of the findings, because clinical relevance depends not only on material behavior under identical geometry but also on benchmarking against established implant-abutment systems.

The primary objective of the present study was therefore to benchmark the load-to-failure performance and post-failure deformation pattern of the experimental Nb-1Zr implant assembly against a commercial Ti-Zr benchmark assembly with a comparable diameter (Straumann® BLX, Roxolid®, SLA®) under standardized restorative conditions. The form-identical Ti6Al4V assembly was retained as an internal material control. To ensure comparability of the loading conditions, the implant axis and crown geometry were standardized across groups, including an adjustment of the abutment height for the commercial system.

The commercial Straumann Ti-Zr assembly was included as a reference benchmark rather than as the primary object of evaluation. Its purpose was to contextualize the mechanical performance of the experimental implants against a clinically established system with the same nominal diameter and a similar implant length. Based on our previous findings, the experimental assemblies were expected to exceed the predefined clinically relevant threshold of 800 N. The following null hypotheses were tested in the new three-group analysis: (1) maximum load to failure (F_{max}) does not differ among the experimental Nb-1Zr assembly, the form-identical Ti-6Al-4V internal control, and the commercial Ti-Zr reference assembly, and (2) mean absolute circumferential deviations do not differ among the three assemblies at the implant shoulder, lower abutment margin, or upper abutment margin.

2 Materials and methods

2.1 Study Design

In this in vitro study, the load-bearing capacity and deformation behavior of two artificially aged experimental implant systems made of Nb-1Zr and Ti-6Al-4V were compared and benchmarked against an established commercially available Ti-Zr implant system, which served as a scale. Each group comprised eight specimens.

In general, all implants were fitted with monolithic zirconia crowns that replicated the occlusal morphology of an upper first molar. Following artificial aging by chewing simulation and thermocycling, the specimens were loaded in a universal testing machine until failure. The three-dimensional deformation of the implant-abutment complex was evaluated by superimposing digital scans taken before aging and after the load test until failure.

The previously published two-group comparison showed that the experimental Nb-1Zr and Ti-6Al-4V assemblies reached mean load-to-failure values of 2595 N ± 1068 N and 2358 N ± 1057 N, respectively, with all specimens exceeding 800 N [11]. Nevertheless, both groups represented form-identical experimental prototypes. To place these findings into a clinically more meaningful context, the present study additionally benchmarks the experimental assemblies against a commercially established Ti-Zr

implant assembly of comparable diameter, representing a system routinely used in clinical practice at our institution.

2.2 Implant Systems

The form identical experimental implants were fabricated from Nb-1Zr and Ti-6Al-4V. They were 14 mm long with a diameter of 4.5 mm. The implants were designed as bone-level implants with a parallel-walled shaft, a flat apical geometry, and an internal conical connection (Fig. 1). The experimental implants have an additional internal chamber, which is assumed to be a reservoir for antiinflammatoric drugs and a miniaturized pumping unit to present the drug through a porous implant surface to the surrounding tissues. Access to this additional internal cavity was considered through the central M2 screw channel; the coronal connection comprised an 80° conical section and an anti-rotational guiding profile.

The Straumann® BLX implant (Ø 4.5 mm RB, SLA®, 16 mm, Roxolid®, Straumann Holding AG, Basel, Switzerland) was selected as a clinically established commercial reference with the same nominal diameter, a similar available implant length, and routine use at our institution and was therefore used for the benchmark group. Because identical conditions could not be achieved between the experimental prototypes and the commercial system, the commercial assembly was adapted as closely as possible to the experimental restorative setup. To ensure identical implant axis and identical load axis, the implant position of the experimental implant was transferred using a custom transfer key. The occlusal reduction of the Straumann abutments about 3.4 mm was determined by analyzing lateral views of the experimental and commercial abutment datasets generated in the same model situation (Fig. 2). On this basis, the commercial abutments were shortened by 3.4 mm using a precision cutting machine (Brillant 220, ATM Qness GmbH, Mammelzen, Germany), and the resulting sharp edges were smoothed using a PowerPro 4000 grinder/polisher (Buehler/ITW Test & Measurement GmbH, Leinfelden-Echterdingen, Germany).

All abutments were screwed into the implants with a torque of 25 Ncm in the experimental implants and with 35 Ncm in the commercial implant system.

2.3 Crown design and specimen preparation

A standardized dental training model (Frasaco AG-3, Frasaco GmbH, Tettnang, Germany) was used to design the implant-supported restoration. Tooth 16 was selected as reference because the occlusal morphology of an upper first molar allows reproducible axial loading. The original tooth morphology was digitized using Primescan and CEREC 5.4 software (Dentsply Sirona, Bensheim, Germany) and transferred to the implant crown by a digital copy-milling workflow.

Separate crown designs were generated for the experimental and commercial implant groups to account for differences in abutment geometry. However, the occlusal morphology was kept identical in all specimens to ensure comparable load application.

In addition to the crowns, which were already examined in our first publication [11], further eight zirconia crowns had to be manufactured for the benchmark group. Because the commercial abutment geometry differed from the experimental abutments, the internal and cervical crown geometry was adapted accordingly, while the occlusal morphology of tooth 16 was kept identical across all groups. For this aim, CEREC 5.4. provides a copy-milling strategy. Therefore, the initial circumferental and occlusal crown design was duplicated and transferred to the Straumann abutment to generate the internal crown geometry.

After sintering according to the manufacturer's instructions, the fit of each crown was checked on the corresponding abutment. No additional adjustment was required. The specimens were embedded in polyurethane-based embedding material using a custom transfer system to ensure identical implant axis and crown orientation. The embedding material was filled up to approximately 2 mm apical to the implant shoulder, leaving the coronal implant region unsupported.

2.4 Cementation and Artificial Aging

According to clinical procedures, the screw access channels were temporarily sealed with Cavit (3M Deutschland GmbH, Neuss, Germany) prior to cementation. The inner surfaces of the zirconia crowns were conditioned with Ceramic Bond (VOCO GmbH, Cuxhaven, Germany), and the crowns were adhesively cemented with SpeedCEM Plus (Ivoclar Vivadent GmbH, Ellwangen, Germany) according to the manufacturer's instructions.

After cementation, all specimens were stored at 36°C for 24 hours. Artificial aging was performed in a chewing simulator (CS-4, SD Mechatronik, Feldkirchen-Westerham, Germany) over 1×10^6 cycles at an axial load regarding the implant axis of 25 N. The load was applied using a stainless steel ball with a diameter of 6 mm. During the chewing simulation, thermocycling between 5°C and 55°C was performed for 4×10^3 cycles.

After artificial aging, the specimens were stored again at 36°C for 24 hours prior to mechanical testing.

2.5. Load-to-failure testing

Load-to-failure testing was performed using a universal testing machine (UTS RetroLine, ZwickRoell GmbH & Co. KG, Ulm, Germany). The specimens were loaded axially on the

occlusal surface of the zirconia crown using a stainless-steel ball with a diameter of 6 mm (Fig. 3).

A preload of 2 N was applied, followed by continuous loading at a crosshead speed of 0.5 mm/min until failure. Failure was defined as fracture of the zirconia crown or a force drop of 20% from the maximum force recorded. Maximum load to failure (F_{max}) and axial displacement at F_{max} were recorded using testXpert software.

2.6 Three-dimensional deformation analysis

For three-dimensional deformation analysis, each specimen was scanned before crown cementation of the crown and again after load-to-failure testing. After mechanical testing, fractured crowns or crown fragments and residual cement were removed, and the implant–abutment complexes were digitized with Primescan (Dentsply Sirona, Bensheim, Germany).

The baseline and post-loading scans were superimposed using OraCheck software (Oracheck 5.0, Dentsply Sirona, Bensheim, Germany). Individual reference markings in the embedding material were used to improve scan alignment.

Deformation was evaluated at three predefined levels: implant shoulder, lower abutment margin, and upper abutment margin to increase sensitivity to subtle positional changes along the supragingival abutment height. At each level, deviations were measured at four circumferential positions: 0°, 90°, 180°, and 270°. For each specimen and measurement level, the absolute deviations recorded at 0°, 90°, 180°, and 270° were converted to absolute values and subsequently averaged, yielding one mean absolute circumferential deviation per specimen. This approach prevented positive and negative deviations from cancelling each other out. In contrast to the previously reported maximum local deviation analysis [11], the present analysis used mean circumferential deviations to characterize the overall post-failure deformation pattern. Deviations were recorded in millimeters (Fig. 4).

2.7 Statistical analysis

Statistical analysis was performed using IBM SPSS Statistics (SPSS V. 29, IBM Corp, Armonk, NY, USA). Descriptive statistics were calculated for F_{max}, axial displacement at F_{max}, and three-dimensional deviations.

Normal distribution and homogeneity of variance were assessed before group comparisons. One-way analysis of variance was used to compare the three groups. Post-hoc pairwise comparisons were performed using Tukey's HSD test. The level of significance was set at $p = 0.05$.

3 Results

3.1 artificial aging

All specimens survived artificial aging by chewing simulation and thermocycling. No crown fracture, crown decementation, screw loosening, or failure of the implant–abutment connection was observed during chewing simulation. Consequently, all specimens were included in the subsequent load-to-failure testing.

3.2 Load-bearing capacity

The highest mean maximum load to failure was recorded in the commercial titanium-zirconium implant group, with 3743.14 N ± 200.83 N. Referring to the previous publication, the experimental Nb-1Zr

implants reached a mean F_{max} of 2594.92 N ± 1068.29 N, whereas the form-identical Ti-6Al-4V implants reached 2358.42 N ± 1057.23 N. The lowest individual failure load was 1367.88 N in the Ti-6Al-4V group. The highest individual value was measured in the Nb-1Zr group, with 4603.49 N [11]. All specimens exceeded the clinically relevant threshold of 800 N [12, 13].

One-way ANOVA revealed a significant difference between the three groups regarding F_{max} ($p = 0.010$). Post-hoc analysis showed that the commercial implant group had significantly higher load-bearing capacity than both experimental groups Nb-1Zr ($p = 0.040$) as well as Ti-6Al-4V ($p = 0.012$). As already known from the previous publication, the experimental groups did not differ significantly ($p = 0.852$) [11].

Axial displacement at F_{max} did not differ significantly between the groups (Table 1, Fig. 5).

Table 1
* Load-to-failure results and axial displacement at Fmax*Data from the Nb-1Zr and Ti6Al4V groups were reported previously [8] and are reproduced here to enable the three-group system-level benchmark analysis.

Nb-1Zr	**n**	**Fmax mean ± SD [N]**	**Minimum [N]**	**Maximum [N]**	**Axial displacement at Fmax mean ± SD [µm]**
	8	**2594.9 ± 1068.3**	**1392.6**	**4603.5**	**823.1 ± 262.0**
Ti-6Al-4V	8	2358.4 ± 1057.2	1367.9	3880.4	695.1 ± 130.1
Commercial Ti–Zr implant	8	3743.1 ± 200.8	3275.2	3911.0	1012.5 ± 334.4

3.3 Failure modes

Failure was defined a priori as fracture of the zirconia crown or a 20% reduction in force after Fmax. Crown fracture occurred in [1/8] Nb-1Zr, [1/8] Ti-6Al-4V, and [0/8] commercial reference assemblies; the remaining specimens met the 20% force-drop criterion without complete crown fracture (Fig. 6). Among specimens with crown fracture, the fracture line generally followed the central fissure in a mesiodistal direction. No implant-body fracture was observed. One commercial abutment fractured directly above the implant shoulder and was excluded from the three-dimensional scan analysis because reliable superimposition was no longer possible.

3.4 Three-dimensional deformation analysis

For Three-dimensional deformation analysis baseline scans obtained before aging were superimposed with post-loading scans obtained after load-to-failure testing. In the commercial implant group, seven specimens were included in this analysis because one abutment fractured during mechanical loading. The data are given in Table 2 and Fig. 7 (Table 2, Fig. 7).

Table 2
Three-dimensional deviations at the implant-abutment complex

		n	Mean ± SD [mm]	Minimum [mm]	Maximum [mm]
Level 1 — implant shoulder	Nb-1Zr	8	0.034 ± 0.023	0.00	0.07
	Ti-6Al-4V	8	0.010 ± 0.008	0.00	0.02
	Commercial Ti–Zr implant	7	0.024 ± 0.021	0.00	0.06
Level 2 — lower abutment margin	Nb-1Zr	8	0.046 ± 0.021	0.02	0.08
	Ti-6Al-4V	8	0.024 ± 0.018	0.00	0.05
	Commercial Ti–Zr implant	7	0.259 ± 0.094	0.09	0.35
Level 3 — upper abutment margin	Nb-1Zr	8	0.076 ± 0.065	0.02	0.21
	Ti-6Al-4V	8	0.070 ± 0.073	0.02	0.20
	Commercial Ti–Zr implant	7	0.287 ± 0.160	0.08	0.58

At the implant shoulder level, level 1, deviations were low in all groups and the overall group comparison narrowly missed statistical significance ($p = 0.054$). In contrast, the commercial implant group showed markedly higher deviations at both abutment levels compared with the two experimental groups. These differences were statistically significant at the lower abutment margin (level 2) ($p < 0.001$) and at the upper abutment margin (level 3) ($p = 0.001$). The three different levels were used, to ensure that even small deformations could be detected, due to the fact, that small radial displacements at level 1 or level 2 will result in higher aberrations at level 3. Post-hoc analysis confirmed significantly higher deformation values for the commercial implant group compared with both Nb-1Zr and Ti-6Al-4V at these levels, whereas no significant differences were detected between the two experimental groups.

The commercial implant group showed visible deformation in the abutment region after loading. In the experimental groups, no macroscopically visible deformation of the abutment body was observed. The more pronounced abutment-level deviations in the commercial reference group must be interpreted in light of the fundamentally different abutment cross-sections. The commercial abutment had a narrower implant-proximal configuration, whereas the experimental abutment geometry was developed to preserve an access pathway into the implant interior and therefore required a different material distribution and wall thickness. Accordingly, the observed deviations describe system-specific post-

failure localization under the tested conditions and should not be interpreted as a direct comparison of the intrinsic deformation resistance or quality of the two abutment designs.

4 Discussion

The present study extends the previously reported two-group material comparison [11] by introducing a commercial Ti-Zr benchmark assembly and evaluating three-group load-to-failure performance and post-failure deformation patterns. The commercial benchmark reached the highest mean F_{max}, whereas the two experimental assemblies remained comparable. Post-failure scans indicated a more pronounced abutment-centered deviation pattern in the commercial benchmark assembly.

This system-level benchmark is relevant to the SIIRI concept because future infection-reactive implant designs require sufficient mechanical reserves despite the internal architecture envisaged for controlled local drug delivery. Under the present conditions, the Nb-1Zr assembly maintained load-bearing capacity above clinically relevant force levels of 800 N [12, 13]. Nb-based alloys remain attractive for implant applications because of their favorable corrosion resistance, biocompatibility, and mechanical properties [7, 8]. Recent material-processing studies further support the development of Nb-1Zr as a high-strength structural material for dental implant applications [14].

The form-identical Ti-6Al-4V assembly served as an internal material control and confirmed the previously reported absence of a significant material-related difference in F_{max} [11]. The substantially greater variability in both experimental groups may partly reflect their non-industrial manufacturing process and should be considered when interpreting the group means. The higher F_{max} of the commercial benchmark should be interpreted as a system-level effect rather than an isolated material effect. Fixture geometry, implant-abutment connection, abutment configuration, screw-joint mechanics, implant length and industrial manufacturing precision differed from the experimental assemblies and may all have contributed to the observed performance.

All assemblies reached F_{max} values above 800 N, indicating substantial reserve relative to reported parafunctional bite forces [12, 13, 15]. Because the anatomically shaped molar crown and axial loading configuration differ from DIN ISO 14801, however, the absolute F_{max} values should be interpreted within this clinically oriented assembly-level test setup and not transferred directly to standardized fatigue data.

The principal new finding was the more pronounced abutment-centered post-failure deviation pattern in the commercial benchmark despite its higher F_{max}. One commercial abutment fractured, whereas no implant body fracture occurred in any group, indicating that failure localized primarily within the supracrestal implant-abutment-crown assembly under the present loading conditions. In the experimental groups, the absence of visible abutment deformation is compatible with a screw-related positional change, but this mechanism was not directly verified. Connection design, abutment geometry, screw-joint mechanics, and the shortened commercial abutment may all have influenced failure

localization [10, 16, 17]. Because scans were obtained after group-specific terminal loads, the measured deviations describe post-failure localization rather than intrinsic deformation resistance.

The embedding design must also be considered when interpreting the deformation results. The implants were embedded with the implant shoulder exposed, leaving the coronal region unsupported. This design was chosen to avoid artificial stabilization of the region where deformation was expected. Clinically, bone-level implants are ideally placed with the implant shoulder at the bone crest; however, peri-implant marginal bone changes may occur over time. Early marginal bone remodeling is a common, non-infective biological process occurring predominantly during the healing and prosthetic phases after implant placement, although its extent varies depending on surgical, prosthetic, and soft-tissue-related factors [18–20]. Furthermore, finite element studies have shown that stress concentration around the implant shoulder and peri-implant bone are influenced by bone loss, implant design, and force direction [21, 22]. Therefore, the present embedding approach represents a mechanically demanding approximation of a partially unsupported crestal region rather than an idealized fully supported implant situation.

Several limitations are particularly relevant to the system-level comparison. The small group size and non-industrial manufacture of the experimental implants limit precision and likely contributed to the wide dispersion of F_{max}. Due to the experimental design of the newly developed implants and to this relevant modifications of their geometry, the commercial benchmark implants differed in material, implant length, connection design, abutment geometry, screw-joint configuration, and manufacturing process. Moreover, its abutment was shortened to approximate the restorative height of the experimental assemblies. The results therefore characterize the complete implant–abutment–crown assemblies rather than isolated material properties or an unmodified clinical commercial configuration. This was necessary to benchmark the experimental implants against the established system, what was the aim of the presented study.

An additional limitation concerns the group-specific crown geometry. Although the occlusal morphology and loading point were standardized, differences in abutment geometry required adaptations of the internal and cervical crown design. Consequently, zirconia wall thickness and crown volume could not be kept identical among groups. Greater crown material thickness in parts of the commercial benchmark restorations may have contributed to the higher load-to-failure values and may have permitted greater force transmission to the abutment before terminal failure, thereby also influencing the observed abutment-centered deviation pattern. Because crown dimensions were not quantitatively analyzed, their contribution cannot be distinguished from the effects of implant–abutment geometry and screw-joint mechanics.

Importantly, the commercial Straumann assembly was not included to evaluate or rank the performance of the Straumann system itself. It only served as a clinically established reference benchmark to determine whether the experimental assemblies achieved load-bearing capacity and post-failure dimensional stability within a mechanically relevant range. The findings should therefore be interpreted

as a translational positioning of the experimental concept relative to an established reference assembly, rather than as a direct product comparison or demonstration of equivalence.

In addition, the experimental abutments and screws were made of Ti-6Al-4V. Component-level analyses, including SEM or micro-computed tomography, are required to determine whether screw deformation, loosening, or interface damage caused the observed positional changes.

Taken together, the commercial benchmark adds translational context to the previously reported material comparison. The findings indicate that assembly design and manufacturing factors must be considered alongside implant material when interpreting system-level mechanical performance.

5 Conclusion

Within the limitations of this in vitro study, the new three-group benchmark analysis revealed significant differences in maximum load to failure among the tested implant–abutment–crown assemblies. Accordingly, the first null hypothesis was rejected: the commercial Ti-Zr reference assembly achieved higher F_{max} values than both experimental assemblies, whereas the previously reported Nb-1Zr and form-identical Ti-6Al-4V assemblies did not differ significantly.

The second null hypothesis was partially rejected. Mean absolute circumferential deviations did not differ significantly among the groups at the implant shoulder but were significantly greater for the commercial reference assembly at both abutment levels after terminal loading. These findings provide a clinically relevant system-level context for the previously reported mechanical performance of the experimental Nb-1Zr assembly. They should not be interpreted as evidence of equivalence or as a direct evaluation of the commercial implant system, because the tested assemblies differed in implant and abutment geometry, screw-joint configuration, crown geometry and wall thickness, manufacturing precision, and terminal load.

Taken together, the findings suggest that the experimental Nb-1Zr implant concept has reached a mechanically meaningful stage of development. Despite manual prototype manufacture and the additional structural demands imposed by the intended local drug-delivery function, its load-to-failure performance and comparatively low post-failure deviations support its continued development toward a standardized and clinically applicable implant–abutment assembly. Further optimization of the implant–abutment design and standardized manufacturing procedures will be required to reduce variability and to confirm the mechanical performance of the final drug-delivery-adapted system.

Declarations

Acknowledgements

This study was funded by the *Deutsche Forschungsgemeinschaf*t (DFG, German Research Foundation) – SFB/TRR-298-SIIRI – Project-ID 426335750.

The authors declare no conflicts of interest.

Author Contribution

K.P. - Experimental investigations, data analysis, statistical evaluation, interpretation of results, and original manuscript draftingJ.-T. S. - Manufacture of experimental Nb-1Zr and Ti-6Al-4V implant prototypes, review and editingC. K. - Manufacture of experimental Nb-1Zr and Ti-6Al-4V implant prototypes, review and editingN. B.-B. - review and editingM. P. - review and editingH. J. M. - Conception of the study, review and editingM. S. - Conception of the study, review and editingP.-C. P. - Conception of the study, data analysis, manuscript preparation, scientific discussion, statistical evaluation and review and editing

Data Availability

All data supporting the findings of this study are available within the paper.

References

1. Chen, L., et al., *Titanium particles in peri-implantitis: distribution, pathogenesis and prospects*. Int J Oral Sci, 2023. 15(1): p. 49.
2. Freitag, L., et al., *Dental implant material related changes in molecular signatures in peri-implantitis - A systematic review and integrative analysis of omics in-vitro studies*. Dental Materials, 2023. 39(1): p. 101–113.
3. Rodriguez Alvarez, M.B., et al., *Release of Titanium Particles After Implantoplasty in the Treatment of Peri-Implantitis: Local and Systemic Implications-An Integrative Systematic Review*. J Clin Med, 2025. 14(24).
4. Toledano-Serrabona, J., et al., *Ion release and local effects of titanium metal particles from dental implants: An experimental study in rats*. J Periodontol, 2023. 94(1): p. 119–129.
5. Mombelli, A., D. Hashim, and N. Cionca, *What is the impact of titanium particles and biocorrosion on implant survival and complications? A critical review*. Clin Oral Implants Res, 2018. 29 Suppl 18: p. 37–53.
6. Dionigi, C., et al., *Titanium micro-particles are commonly found in soft tissues surrounding dental implants*. Commun Med (Lond), 2025. 5(1): p. 78.
7. Liu, Z., et al., *Bio-functional niobium-based metallic biomaterials: Exploring their physicomechanical properties, biological significance, and implant applications*. Acta Biomater, 2025. 192: p. 1–27.
8. Safavi, M.S., et al., *Progress in Niobium Oxide-Containing Coatings for Biomedical Applications: A Critical Review*. ACS Omega, 2022. 7(11): p. 9088–9107.
9. Sammour, S.R., et al., *Impact of implant abutment connection designs and cyclic loading on screw stability in dental implants: A systematic review and meta-analysis.* J Prosthet Dent, 2026. 135(2): p. 317.e1-317.e14.

10. Lorusso, F., et al., *Microleakage and mechanical behavior of conical vs. internal hexagon implant-abutment connection under a cyclic load fatigue test*. Eur Rev Med Pharmacol Sci, 2023. 27(3 Suppl): p. 122–127.
11. Pott, P.C., et al., *Load-bearing capacity of an experimental dental implant made of Nb-1Zr*. J Mater Sci Mater Med, 2025. 36(1): p. 12.
12. Cosme, D.C., et al., *Bruxism and voluntary maximal bite force in young dentate adults*. Int J Prosthodont, 2005. 18(4): p. 328–332.
13. Chrcanovic, B.R., et al., *Bruxism and dental implant failures: a multilevel mixed effects parametric survival analysis approach*. J Oral Rehabil, 2016. 43(11): p. 813–823.
14. Schleich, J.T., et al., *Co-extrusion of Nb-1Zr Powder for the Production of a Biocompatible High-Strength Material for Dental Implants*. Advanced Engineering Materials, 2024. 26(22): p. 2401436.
15. Steiner, M., et al., *In vitro evaluation of a mechanical testing chewing simulator*. Dent Mater, 2009. 25(4): p. 494–499.
16. Camps-Font, O., et al., *Comparison of external, internal flat-to-flat, and conical implant abutment connections for implant-supported prostheses: A systematic review and network meta-analysis of randomized clinical trials*. J Prosthet Dent, 2023. 130(3): p. 327–340.
17. Hendi, A., S. Mirzaee, and M. Falahchai, *The effect of different implant-abutment types and heights on screw loosening in cases with increased crown height space*. Clin Exp Dent Res, 2024. 10(3): p. e894.
18. Monje, A., et al., *Influence of buccal bone wall thickness on the peri-implant hard and soft tissue dimensional changes: A systematic review*. Clinical Oral Implants Research, 2023. 34(3): p. 157–176.
19. Lombardi, T., et al., *Factors Influencing Early Marginal Bone Loss around Dental Implants Positioned Subcrestally: A Multicenter Prospective Clinical Study*. J Clin Med, 2019. 8(8).
20. Cochran, D.L., et al., *A prospective multicenter 5-year radiographic evaluation of crestal bone levels over time in 596 dental implants placed in 192 patients*. J Periodontol, 2009. 80(5): p. 725–33.
21. Jafarian, M., F.S. Mirhashemi, and N. Emadi, *Finite element analysis of stress distribution around a dental implant with different amounts of bone loss: An in vitro study*. Dent Med Probl, 2019. 56(1): p. 27–32.
22. Akbas, O., A. Greuling, and M. Stiesch, *The effects of different grading approaches in additively manufactured dental implants on peri-implant bone stress: A finite element analysis*. J Mech Behav Biomed Mater, 2024. 154: p. 106530.

Figures

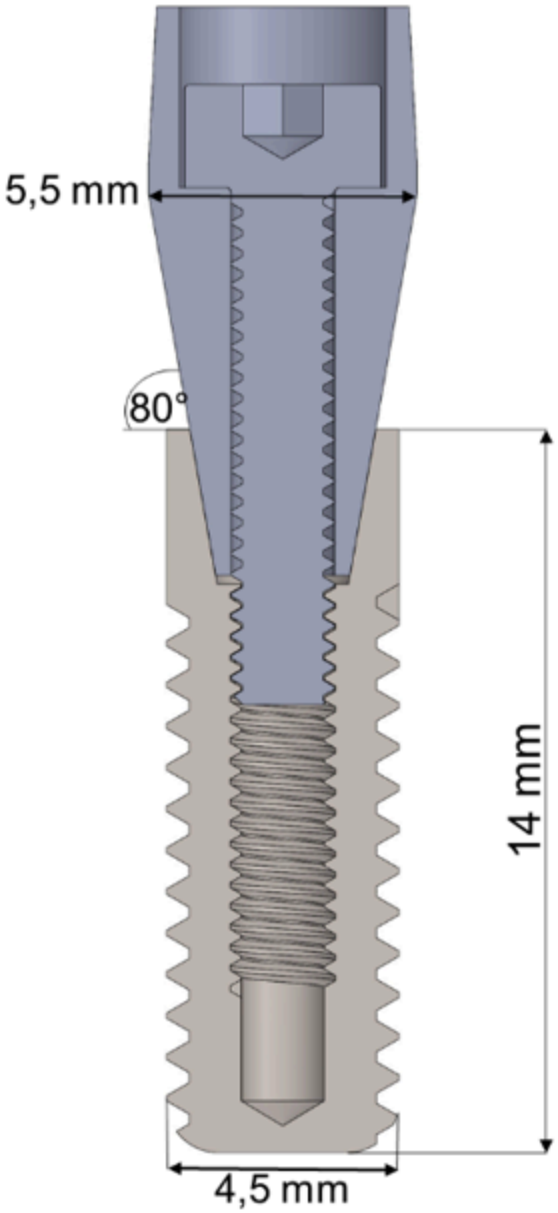


Figure 1

Schematic drawing of the experimental implants geometry and internal structure

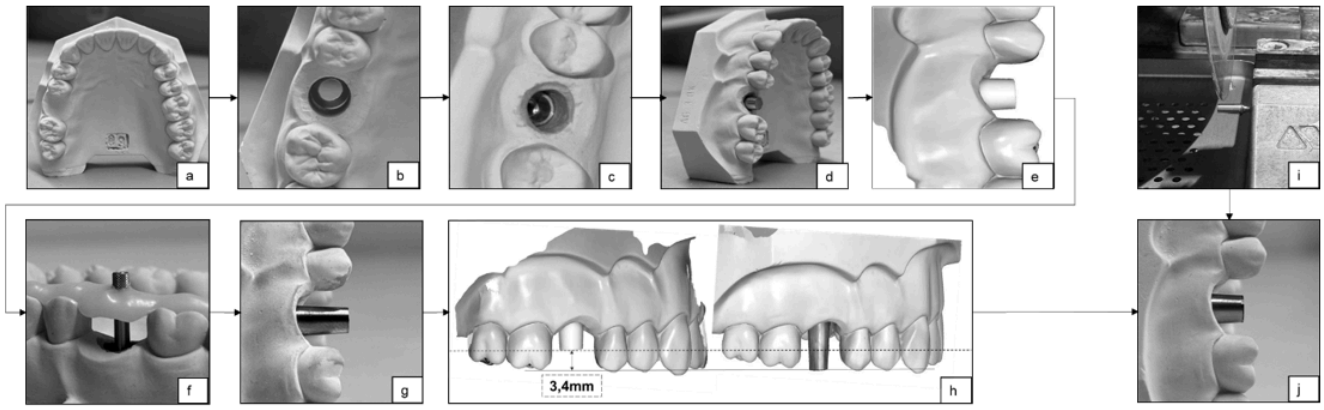


Figure 2

Workflow for implant positioning and abutment shortening process. a) removal of tooth 16 from the maxillary training model; b) preparation of the artificial implant socket; c) embedding of the experimental implant; d) insertion of the experimental abutment; e) lateral view of the experimental abutment; f) fabrication of the positioning transfer key; g) positioning of the Straumann BLX implant; h) digital comparison of abutment heights to determine the required 3.4-mm reduction; i) precision shortening of the commercial abutment; j) commercial abutment after shortening.

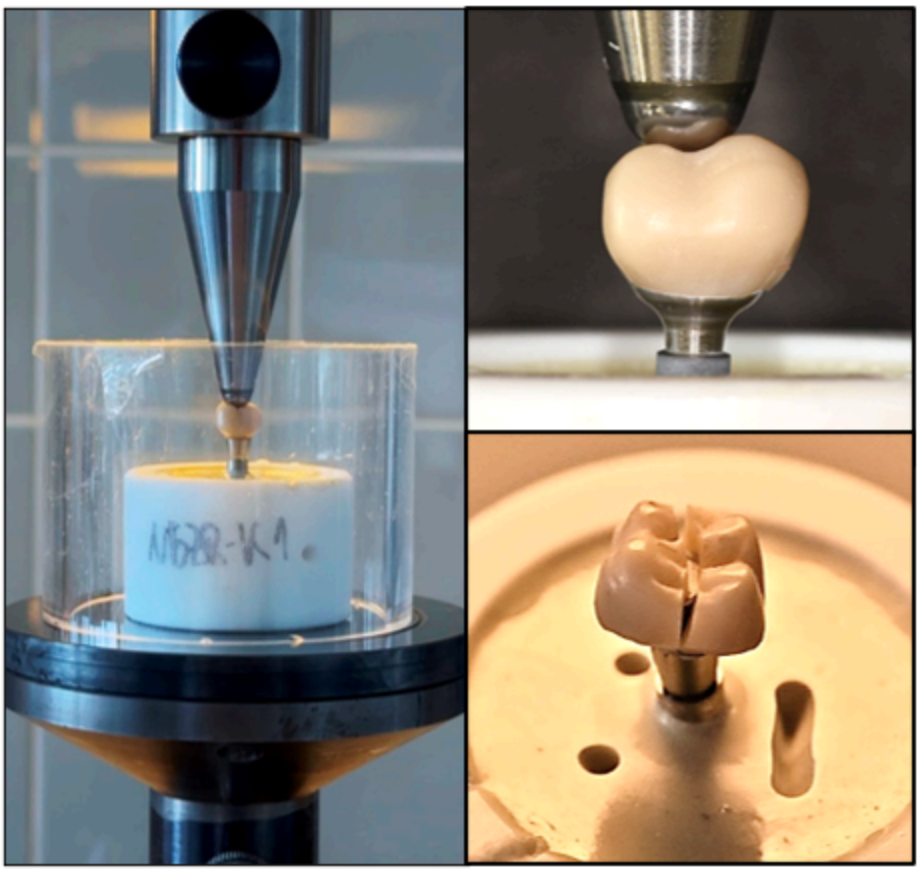


Figure 3

Specimen in Universal Testing Machine during and after load application

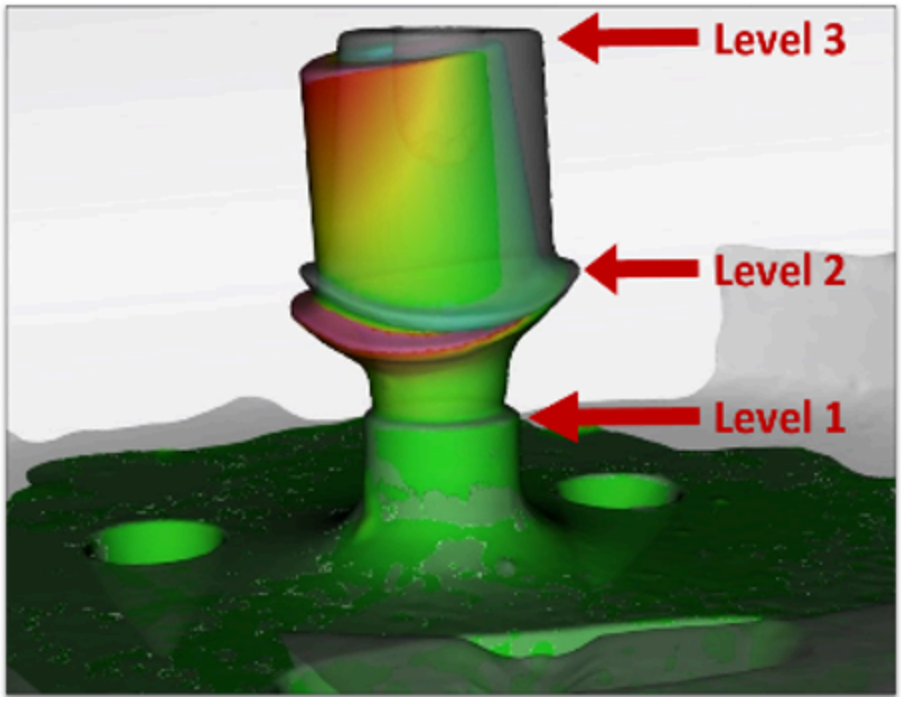


Figure 4

Superimposed abutment of the benchmark group with deviations at levels 1, 2 and 3 after loading.

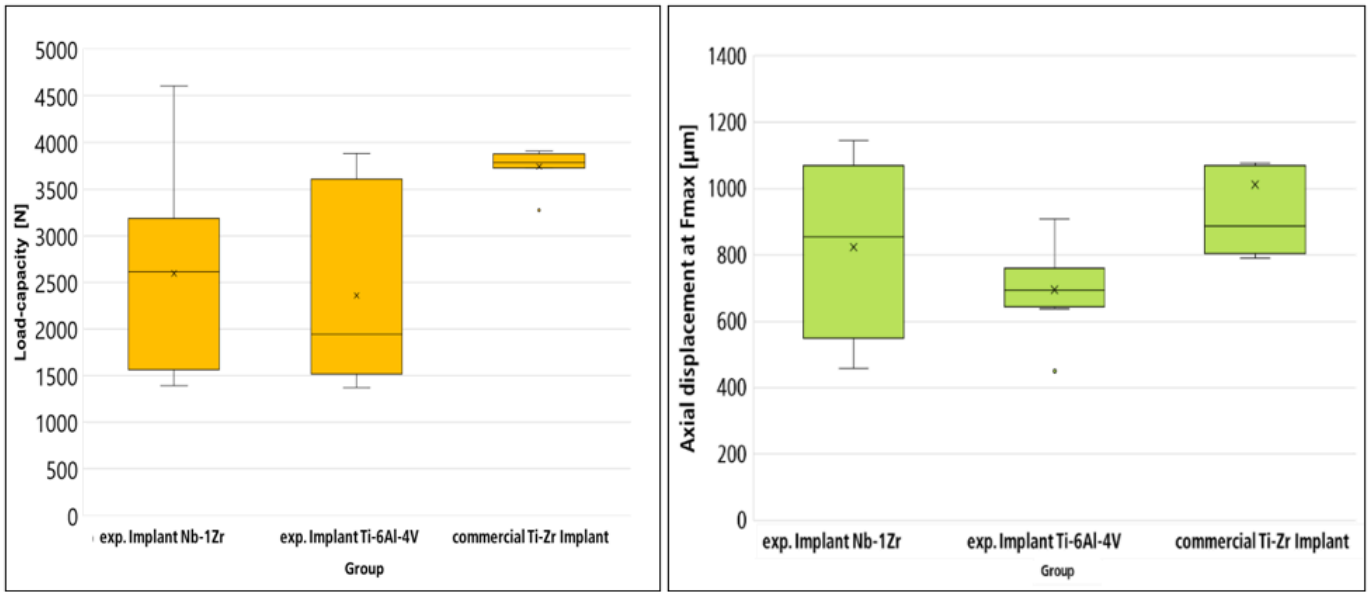


Figure 5

boxplots of the load-capacity (left) and axial displacement (right)

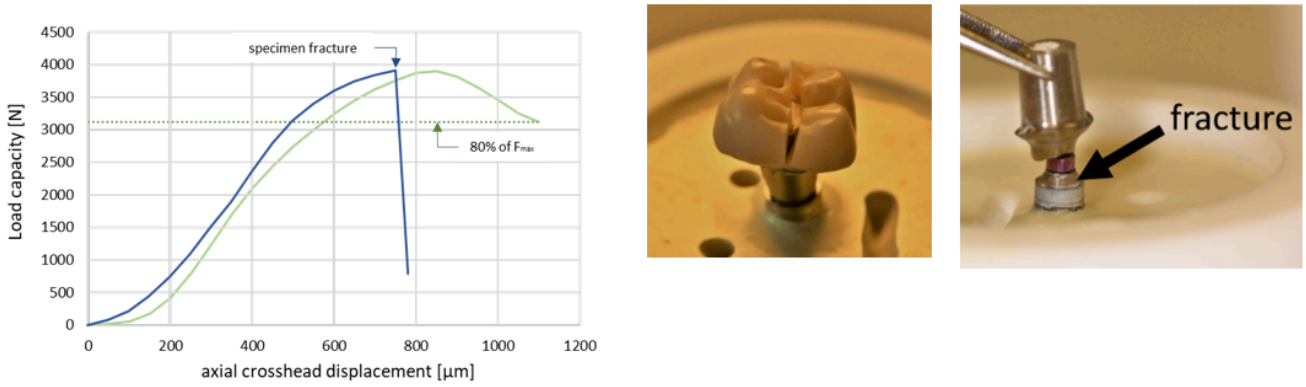


Figure 6

force-displacement plot (left), fractured crown (middle) and fractured abutment (right)

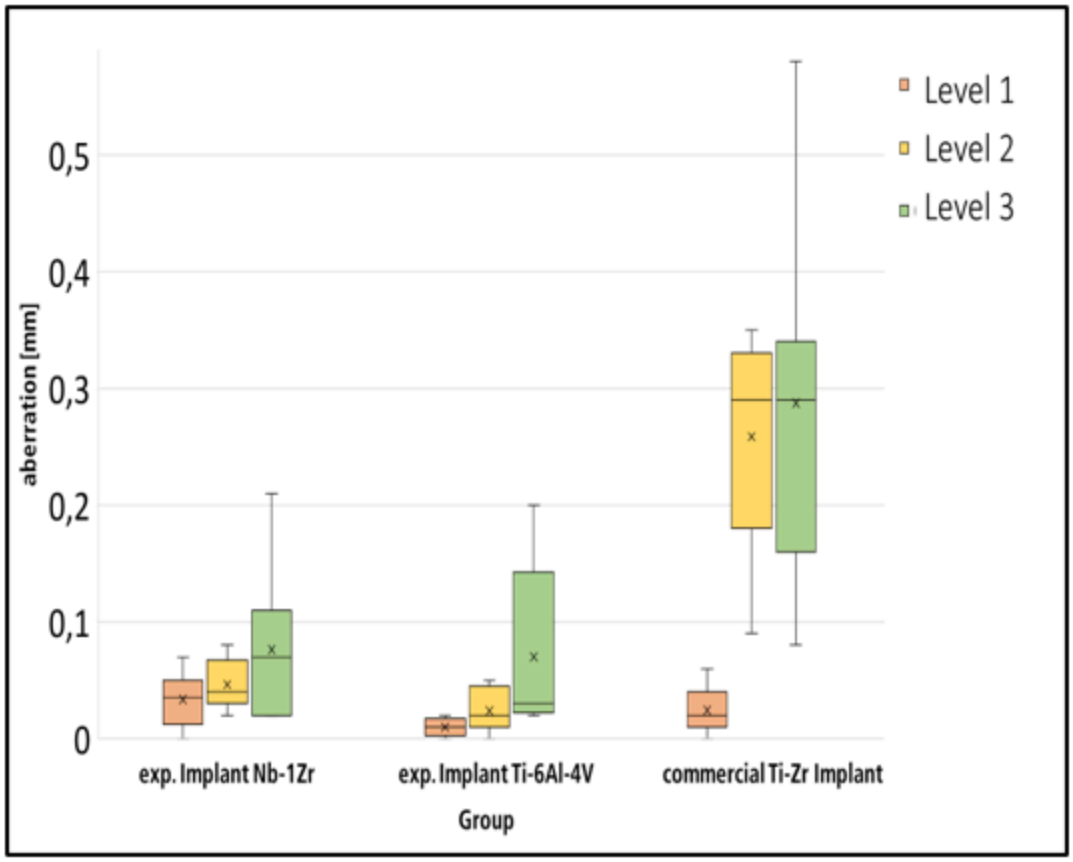


Figure 7

Boxplot of the 3D-aberration at levels 1, 2 and 3

Supplementary Files

This is a list of supplementary files associated with this preprint. Click to download.

- Graphicalabstract.jpg